Asian Journal of Chemistry; Vol. 38, No. 7 (2026), 1696-1706
ASIAN JOURNAL OF CHEMISTRY
https://doi.org/10.14233/ajchem.2026.35910

# Synthesis, Characterisation, Biological Activity and Molecular Docking of Metal(II) Complexes with Schiff Base Derived from *o*-Vanillin and 4-Chloro-*o*-phenylenediamine

ASHOK SINGH[1], MANJU YADAV[2], KULDEEP KUMAR[2], SHIVAM MAURYA[2], SAURABH KUMAR SINGH[3], JAYA DWIVEDI[4] and NAND LAL[1,*]

[1]Department of Chemistry, V.S.S.D. College, Kanpur-208002, India
[2]Department of Chemistry, Maharana Pratap Government P.G. College, Hardoi-241001, India
[3]Department of Chemistry, Lucknow University, Lucknow-226007, India
[4]Department of Chemistry, Banasthali Vidyapeeth, Banasthali-304022, India

*Corresponding author: E-mail: drnandlal71@gmail.com

*Received*: 9 March 2026 *Accepted*: 6 May 2026 *Published online*: 3 July 2026 AJC-22395

This work reports the synthesis, structural elucidation and characterization of the tetradentate Schiff base $H_2L$ (*bis*[3-methoxy-salicylidene]-4-chloro-*o*-phenylenediamine) and its Cu(II) and Ni(II) coordination compounds, respresented as CuL and NiL, respectively. The Schiff base $H_2L$ was synthesized *via* condensation of *o*-vanillin and 4-chloro-*o*-phenylenediamine in a 2:1 molar ratio. The ligand and its Cu(II) and Ni(II) complexes were characterized using elemental analysis, ESI-MS, HRMS, FTIR, UV-visible, $^1$H NMR, $^{13}$C NMR spectroscopy and thermogravimetric analysis (TGA). Molar conductance measurements confirmed the non-electrolytic nature of both complexes in solution. Based on the spectroscopic and analytical data, the CuL and NiL complexes were assigned distorted square-planar geometries. Powder X-ray diffraction (PXRD) and scanning electron microscopy (SEM) were employed to investigate their crystallinity and surface morphology. The antimicrobial potential of $H_2L$, CuL and NiL was evaluated *in vitro* using the agar well diffusion method and *in silico* through molecular docking studies against target proteins from *Escherichia coli* (PDB ID: 1KZN), *Pseudomonas aeruginosa* (PDB ID: 4CL6), *Staphylococcus aureus* (PDB ID: 3FYV) and *Candida albicans* (PDB ID: 5FSA). The results were further correlated with the experimentally determined antimicrobial activities.

**Keywords: Schiff base, Metal(II) complex, Spectral studies, Biocidal efficacy, Molecular docking.**

## INTRODUCTION

The rapid emergence and spread of antimicrobial resistance have become a major challenge for healthcare systems worldwide, creating an urgent need for the development of new and effective therapeutic agents [1]. In this context, metal based compounds have attracted considerable attention owing to their diverse mechanisms of action and promising antimicrobial properties [2]. Among the various classes of bioactive molecules, Schiff bases constitute an important group of ligands due to their straightforward synthesis, structural versatility and wide-ranging biological activities [3,4]. Salicylaldehyde-derived Schiff bases, in particular, have been extensively investigated as polydentate ligands capable of coordinating metal ions in either neutral or deprotonated forms [5].

The biological performance of Schiff bases can be significantly influenced by the nature of substituents present on the aromatic ring. Previous studies have shown that halogen-substituted Schiff bases and their metal complexes often exhibit enhanced antimicrobial activity compared to unsubstituted analogues [6]. The presence of the azomethine group, containing a lone pair of electrons on the $sp^2$-hybridized nitrogen atom, facilitates strong coordination with metal ions, especially when additional donor atoms such as oxygen are present within the ligand framework [7-10]. Chelation generally enhances the lipophilicity of metal complexes, thereby improving their ability to penetrate microbial cell membranes and interact with intracellular biomolecules and enzymes [11].

Beyond their biological importance, Schiff base metal complexes have found applications in catalysis including alkene hydrogenation and ring-opening polymerization reactions, as well as in medicinal and therapeutic fields [12-15]. Schiff bases derived from *o*-vanillin are particularly attractive since they possess additional methoxy and phenolic functionalities that

can contribute to antioxidant, antimicrobial, antifungal and anticancer activities [16]. Furthermore, tetradentate ONNO donor Schiff bases coordinated with transition metals frequently form stable chelate systems exhibiting enhanced biological properties, a phenomenon that can be explained by chelation theory and Overton's concept [17,18].

Copper and nickel are biologically important transition metals that exhibit diverse coordination behaviour and readily form stable metal complexes with multidentate ligands [19]. Owing to their variable coordination geometries and favourable electronic properties, Cu(II) and Ni(II) Schiff base complexes have attracted considerable attention for biomedical, catalytic and electrochemical applications. Previous studies have demonstrated that Ni(II) and Cu(II) complexes containing O,N-donor Schiff bases possess significant antibacterial, antifungal and anticancer activities. For instance, Bahron *et al*. [20,21] reported that Ni(II) complexes of ONNO donor Schiff bases exhibited notable antimicrobial efficacy, while related Cu(II) and Ni(II) complexes showed promising cytotoxic activity against human colorectal carcinoma (HCT116) and Ehrlich ascites carcinoma (EAC) cell lines [20,21]. In addition, Sanatkar *et al*. [22] demonstrated the applicability of a Ni(II) Schiff base complex as an electrochemical sensor for hydrazine detection, highlighting the multifunctional potential of such coordination compounds.

These findings suggest that Schiff bases containing multiple donor atoms in close proximity to the azomethine group can enhance metal coordination and subsequently improve biological performance. Despite the growing interest in Schiff base metal complexes, halogen-substituted tetradentate ONNO donor systems remain relatively underexplored. Therefore, the present work focuses on the synthesis of a novel halogenated tetradentate Schiff base derived from *o*-vanillin and 4-chloro-*o*-phenylenediamine, together with its Cu(II) and Ni(II) complexes. The synthesized compounds were characterized using elemental analysis, FTIR, UV-visible spectroscopy, NMR spectroscopy, mass spectrometry and thermogravimetric analysis to establish their structural features. Furthermore, PXRD and SEM analyses were employed to investigate their crystallinity and surface morphology. The antimicrobial potential of the Schiff base ligand and its metal(II) complexes was evaluated through both *in vitro* biological assays and *in silico* molecular docking studies against selected bacterial and fungal targets.

## EXPERIMENTAL

All chemicals utilised in the present research work were of analytical research grade and were used without further purification. 4-Chloro-*o*-phenylenediamine, hydrated nickel chloride ($NiCl_2 \cdot 2H_2O$), copper acetate hydrate [$Cu(OAc)_2 \cdot H_2O$)] and anhydrous calcium(II) chloride ($CaCl_2$) were acquired from Sigma-Aldrich, USA. Ethanol, ethyl acetate, dimethyl formamide, diethyl ether and other solvents used in synthesis were acquired from Merck Ltd., India and used as purchased.

The melting/decomposition temperatures of the synthesised Schiff base ($H_2L$) and its Cu(II) and Ni(II) complexes were determined using an Ambassador melting point apparatus. UV-visible spectra (200-800 nm) were recorded in DMF using a Hitachi Perkin-Elmer Lambda spectrometer. FTIR spectra were obtained on a Perkin-Elmer Spectrum IR spectrometer. $^1$H and $^{13}$C NMR spectra were recorded in DMSO-$d_6$ on a Bruker 300 MHz spectrometer using tetramethylsilane (TMS) as the internal reference. Thermogravimetric analysis (TGA) was carried out using a Trios thermal analyzer (Version 5.7.0.56). Molar conductance measurements were performed in DMSO ($1 \times 10^{-5}$ M) at room temperature using a Systronic conductivity meter. Magnetic susceptibility measurements were conducted using a Gouy balance. Powder X-ray diffraction (PXRD) patterns were recorded on a Bruker D8 Advance Eco diffractometer, while surface morphology was examined using a JEOL JSM-6490LV scanning electron microscope (SEM). Molecular docking studies were performed using the CB-Dock 2 platform and antimicrobial activity was evaluated by the agar well diffusion method.

**Synthesis of Schiff base [*bis*(3-methoxysalicylidine)-4-chorophenylene-1,2-diamine] ($H_2L$):** An ethanolic solution of *o*-vanillin (3.042 g, 20 mmol) and 4-chloro-*o*-phenylenediamine (1.426 g, 10 mmol) was prepared separately. These solutions are mixed dropwise with continuous stirring and refluxed at 60-80 ºC for 3 h. The progress of the reaction was determined by TLC in *n*-hexane and ethyl acetate. The saffron brown coloured solid was filtered off, washed with ethanol (3 × 10 mL) and diethyl ether. Yield: 3.2 g (78%). m.p.: 224 ºC; Elemental analysis of $C_{22}H_{19}ClN_2O_4$: C, 64.31 (63.92); H, 4.66 (5.72); N, 6.82 (6.94); Cl, 8.63 (8.21); O, 15.58 (15.25); MS (ESI): *m/z* for $H_2L$ ($C_{22}H_{19}ClN_2O_4$): $M^+$ 410.1; $^1$H NMR (300 MHz, DMSO-$d_6$, δ ppm): 12.8 (s, 1H, -OH), 12.7 (s, 1H, -OH), 8.97 (s, 1H, -CH=N), 8.93 (s, 1H, -CH=N), 7.7-6.8 (m, ArH), 3.9 (s, 6H, $OCH_3$); $^{13}$C NMR (75 MHz, DMSO-$d_6$, δ ppm): 165.91, 162.51 (CH=N), 151.02, 150.94, 148.33, 143.83, 141.67 (Ar-N, Ar-O), 132.17, 127.76, 124.32, 124.17, 121.82, 120.17, 119.79, 119.75, 119.18, 117.98, 116.11, 115,98 (Ar-CH, ArC, C-Cl), 56.11, 56.2 ($OCH_3$); UV-Vis (DMF, $1 \times 10^{-3}$ M, nm): 290 ($\pi \rightarrow \pi^*$), 340 ($n \rightarrow \pi^*$). FTIR (KBr, $\nu_{max}$, $cm^{-1}$): 3363 (O-H), 3067 (Ar-H), 2947 (aliph. C-H), 1611 (-C=N), 1575 (C=C), 1252 (C-O); molar conductance in DMSO ($1.0 \times 10^{-5}$ M): 9.8 $\Omega^{-1}$ $cm^2$ $mol^{-1}$.

**Synthesis of metal(II) complexes (CuL and NiL):** The Cu(II) and Ni(II) complexes were synthesized by reacting the Schiff base ligand ($H_2L$) with the corresponding metal salts in a 1:1 molar ratio. In a typical procedure, metal(II) salt was dissolved in methanol (25 mL) under continuous stirring. A preheated methanolic solution of $H_2L$ containing a few drops of triethylamine was then added dropwise to the metal salt solution. The resulting reaction mixture was stirred at 60 ºC for 3 h to facilitate complex formation. Upon cooling to room temperature, the precipitated metal(II) complexes were filtered, washed thoroughly with methanol (3 × 10 mL) followed by diethyl ether (for NiL) or *n*-hexane/diethyl ether (for CuL) and finally dried under vacuum (**Scheme-I**).

**Cu(II) complex (CuL):** Dark brown solid, yield: 77%, m.p.: 233 ºC (decomp.). Elemental analysis of $C_{22}H_{17}ClN_2O_4Cu$ (m.w.: 470.3 g/mol): C, 55.94 (55.31); H, 3.63 (3.93); N, 5.93 (5.89); Cl, 7.50 (7.03); O, 13.69 (13.93); Cu, 13.45 (13.96).

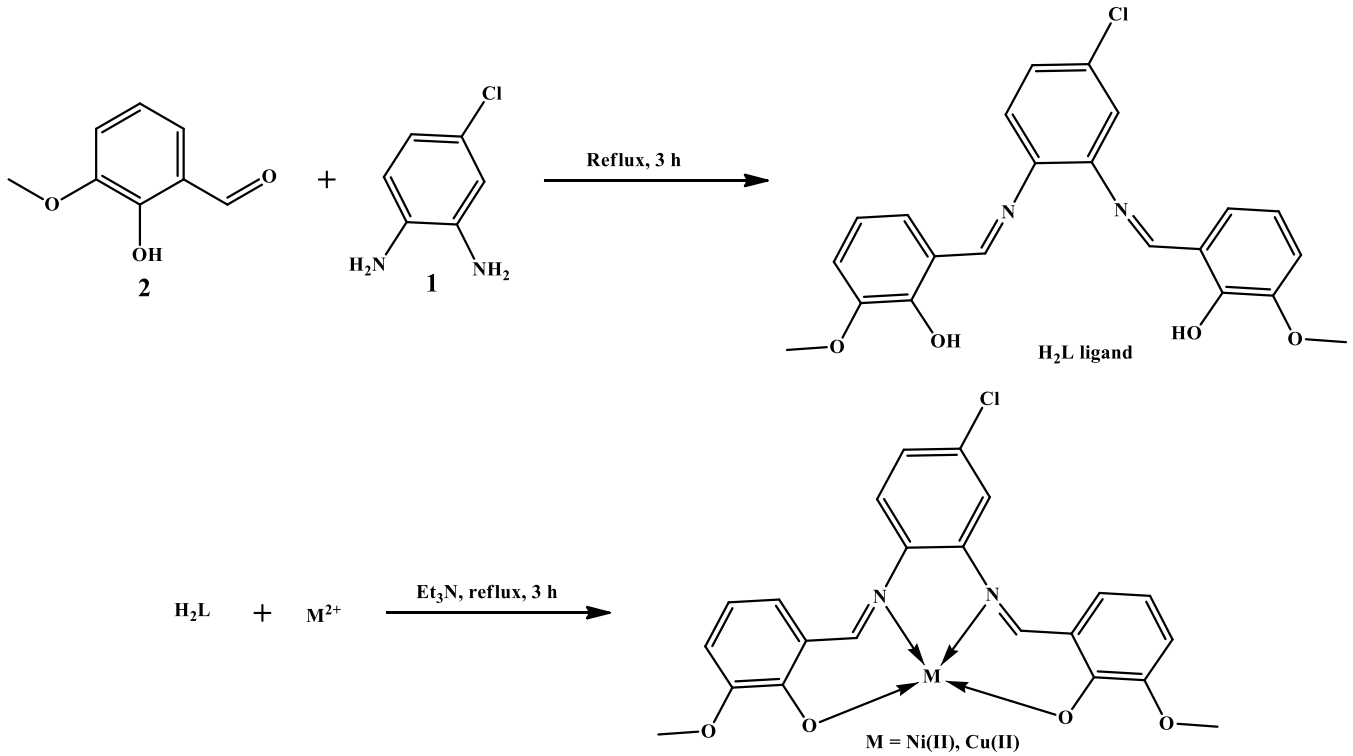


**Scheme-I:** Synthetic route of $H_2L$, CuL and NiL

**Ni(II) complex (NiL):** Blackish-brown solid, yield: 71%, m.p.: 231 ºC (decomp.). Elemental analysis of $C_{22}H_{17}ClN_2O_4Ni$ (m.w.: 465.4 g/mol): C, 56.52 (55.92); H, 3.63 (3.89); N, 5.99 (6.11); Cl, 7.58 (7.70); O, 13.69 (13.29); Ni, 12.55 (13.02).

## Antimicrobial activity

**Antibacterial assay:** The synthesized Schiff base ligand ($H_2L$) and its metal(II) complexes were evaluated for their antibacterial activity against *Escherichia coli* (MTCC 433), *Pseudomonas aeruginosa* (MTCC 2474) and *Staphylococcus aureus* (MTCC 9886) using the agar well diffusion method [23]. Fresh bacterial cultures were uniformly swabbed onto sterile nutrient agar plates, and wells were loaded with solutions of the test compounds (100 µg/mL) prepared in DMSO. Erythromycin at the same concentration was employed as the reference antibacterial agent, while DMSO served as the negative control. The inoculated plates were incubated at 37 ºC for 24 h, after which the antibacterial activity was assessed by measuring the diameter of the inhibition zone (IZD, mm) around each well. The antimicrobial efficacy of the synthesised compounds was evaluated by comparing their inhibition zone diameters with that of the standard drug.

**Antifungal assay:** The antifungal activity of the Schiff base ligand ($H_2L$) and its metal(II) complexes (CuL and NiL) was evaluated against *Candida albicans* (MTCC 228) and *Aspergillus flavus* (MTCC 3682) using the agar well diffusion method, with fluconazole employed as the reference antifungal drug [24]. Sabouraud dextrose agar (SDA) medium was prepared, sterilized by autoclaving at 121 ºC and poured into sterile Petri dishes. Fungal inocula were standardized to 0.5 McFarland turbidity using sterile 0.85% saline solution. The standardized fungal suspension was uniformly spread over the SDA plates to obtain a confluent fungal lawn. Wells of 4 mm diameter were aseptically punched into the agar and filled with different concentrations of the test compounds dissolved in DMSO. The plates were incubated at 35 ºC for 48 h, after which the antifungal activity was assessed by measuring the diameter of the inhibition zones (IZD, mm) surrounding each well. The antifungal efficacy of the synthesized compounds was determined by comparison with the standard drug fluconazole.

**Molecular docking studies**: Molecular docking was employed to investigate the binding interactions and affinities of the synthesized Schiff base ligand ($H_2L$) and its metal(II) complexes with selected microbial target proteins at the molecular level. The study aimed to correlate the observed antimicrobial activity with the ability of the compounds to interact with biologically relevant protein targets. Docking simulations were performed against proteins from *Escherichia coli*, *Pseudomonas aeruginosa*, *Staphylococcus aureus* and *Candida albicans*. The selected protein receptors included the clorobiocin-bound protein from *E. coli* (PDB ID: 1KZN) [25], the target protein from *P. aeruginosa* (PDB ID: 4CL6), the dihydrofolate reductase (DHFR) enzyme from *S. aureus* (PDB ID: 3FYV), which catalyzes the NADPH-dependent reduction of dihydrofolate [26] and the lanosterol 14α-demethylase enzyme from *C. albicans* (PDB ID: 5FSA), a key protein involved in fungal sterol biosynthesis [25]. The Schiff base ligand and metal(II) complexes were docked into the active sites of the selected receptors using the CB-Dock2 server. Binding affinity scores (kcal $mol^{-1}$) were calculated for the highest-ranked binding cavity and the resulting protein–ligand interactions were analyzed to evaluate the potential antimicrobial mechanisms of the synthesized compounds.

## RESULTS AND DISCUSSION

The physical properties and elemental analysis results of the synthesized Schiff base ligand ($H_2L$) and its metal(II) complexes were consistent with the proposed molecular compositions. The experimentally determined carbon, hydrogen and nitrogen contents showed good agreement with the calculated values, confirming the successful synthesis and purity of the compounds. Furthermore, the metal(II) complexes exhibited higher decomposition temperatures than the free ligand, indicating enhanced thermal stability upon coordination. This increased stability can be attributed to the formation of strong metal–ligand bonds and the greater rigidity imparted by chelation within the coordination framework [27].

**UV-vis absorption spectra:** The Schiff base ligand displays a pronounced intense band at 286 nm due to π→π* electronic transitions of the aromatic rings. The azomethine (CH=N) functional group displays a spectral band arising from n→π* transitions at 334 nm [28] (Fig. 1). Complexation of the ligand results in a red shift attributed to the lowering of antibonding molecular orbital energies. Consequently, π→π* transitions in CuL complex are observed at 308 nm, while n→π* transition band is observed at approximately 342 nm. The broad hump centered around 450-550 nm is the most diagnostic feature of the copper(II) complex. This band represents *d-d* transition. The position and width of this band suggest a square planar geometry of CuL complex [29]. Similarly, π→π* transition band in NiL complex is observed at 346 nm and n→π* transition band occurs at 382 nm (Table-1). The nickel(II) complex decreases sharply after 400 nm and remains relatively flat since *d-d* transitions in Ni(II) complexes are often Laporte forbidden and do not appear in the spectra. The lack of a strong, distinct peak in the 500-700 nm range can sometimes suggest a square planar geometry for Ni(II) complexes. The electronic spectra of NiL and CuL complexes display slight wavelength shifts as compared to the free ligand $H_2L$. This observation confirms the coordination of the nitrogen donor site of $H_2L$ with the metal centre [30,31].

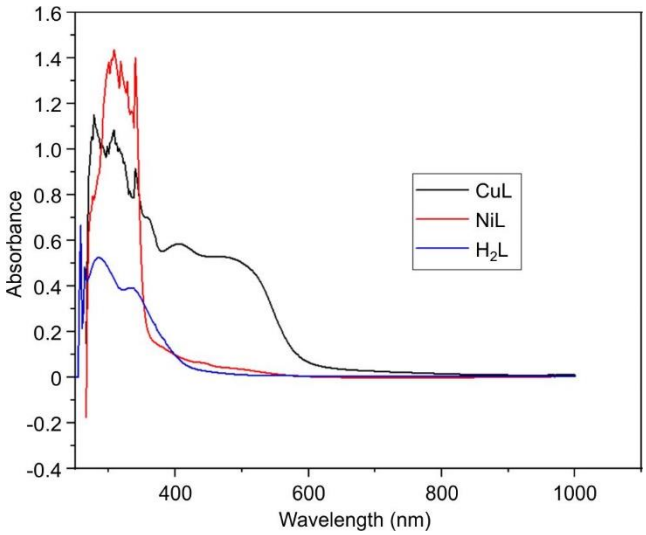


Fig. 1. UV-Vis absorption spectra of ligand and complexes

**Molar conductance and magnetic moment:** Molar conductance measurements of the Cu(II) and Ni(II) complexes were carried out in DMSO ($10^{-5}$ M) at room temperature. The observed conductance values of 19.03 and 9.50 ($\Omega^{-1}$ cm$^2$ mol$^{-1}$ for CuL and NiL, respectively, are characteristic of non-electrolytic species [32]. These low conductivity values indicate the absence of dissociable counter ions in solution, suggesting that the anions are coordinated within the metal coordination sphere rather than existing as free ions [33].

The magnetic behaviour of synthesised metal(II) complexes was investigated using susceptibility measurements performed at room temperature. The Ni(II) complex was found to be diamagnetic with a magnetic moment of 0 BM, which is consistent with a square-planar geometry. The Cu(II) complex exhibited a magnetic moment of 1.41 B.M., corresponding to the presence of one unpaired electron and supporting a distorted square-planar coordination environment around the Cu(II) centre. These results are in-agreement with the proposed structures of the synthesized metal complexes.

**Infrared spectral analysis:** The IR spectra of the ligand $H_2L$ and NiL, CuL complexes are shown in Fig. 2 and provide evidence for the presence of various functional groups [34]. In $H_2L$, a band at 3363 cm$^{-1}$ and a high intensity band at 1611 cm$^{-1}$ were observed, representing ν(O-H) and ν(C=N) stretching, respectively [35]. The position of ν(C=N) band was shifted downward at 1609 cm$^{-1}$ in CuL and 1605 in NiL complex, respectively [20]. This decrease in IR frequencies shows weakening of C=N bond as a result of a decrease in the force constant of the respective bond (Table-2). This shift is attributed to the coordination of the azomethine nitrogen atom with the metal ion through donation of its lone pair of electrons, resulting in the formation of a stable metal–nitrogen coordinate bond. In $H_2L$, moderate-intensity signal observed at 1252 cm$^{-1}$ corresponds to the ν(C–O) vibration of the phenolic moiety, however, it was rather shifted to lower wavenumbers

TABLE-1
UV-VIS ABSORPTION SPECTRA, MAGNETIC MOMENT AND MOLAR CONDUCTIVITY OF $H_2L$ AND NiL, CuL COMPLEXES

| Ligands/complexes | Absorbance (nm) | Assignments | $\mu_{eff}$ (BM) | Molar conductance (Ohm$^{-1}$ cm$^{-2}$ mol$^{-1}$) |
|---|---|---|---|---|
| $H_2L$ | 286 | n→π* | – | – |
| | 334 | n→π* | | |
| NiL | 302 | π→π* | 0.0 | 9.50 |
| | 382 | n→π* | | |
| CuL | 278 | π→π* | 1.41 | 19.03 |
| | 342 | n→π* | | |
| | 408 | LMCT | | |
| | 450-550 | *d–d* transition | | |

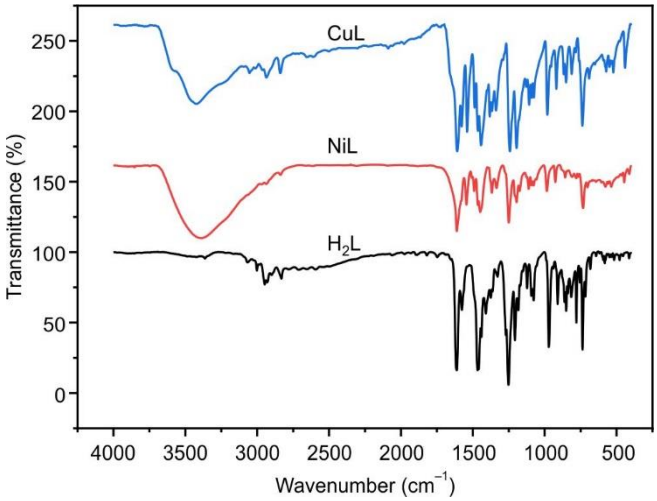


Fig. 2. IR spectra of ligand $H_2L$ and CuL, NiL complexes

at 1242 $cm^{-1}$ in CuL and 1248 $cm^{-1}$ in NiL [36]. This shifting of the ν(C-O) phenolic peak confirms the participation of phenolic oxygen in chelation. Coupled modes of ν(C=N) + ν(C=C) + ν(C-C) can be identified by two bands in CuL at 1540 $cm^{-1}$ and 1490 $cm^{-1}$ that are absent in the spectra of $H_2L$ [37,38]. The complex formation is supported by the appearance of the weak ν(M-O) and ν(M-N) bands in CuL at 523 and 441 $cm^{-1}$ and at 537 $cm^{-1}$ and 447 $cm^{-1}$ in NiL complex [39,40].

**NMR spectral analysis:** The $^1$H NMR spectrum of $H_2L$ (Fig. 3a) exhibited characteristic singlets at δ 12.82 and 12.75 ppm, which were assigned to the phenolic hydroxyl (Ar–OH) protons involved in intramolecular hydrogen bonding. The azomethine (–CH=N–) protons appeared as singlets at δ 8.97 and 8.93 ppm, confirming the formation of the Schiff base framework [41]. The aromatic protons resonated as multiplets in the region δ 6.92-7.62 ppm, while the methoxy protons appeared as a singlet at δ 3.82 ppm. The $^{13}$C NMR spectrum of $H_2L$ (Fig. 3b) further supported the proposed structure. Signals observed at δ 165.89 and 165.70 ppm were assigned to the azomethine carbon atoms (–CH=N–) [42,43]. The resonances at δ 151.02, 150.94, 148.33, 143.83 and 141.67 ppm correspond to aromatic carbons bonded to oxygen and nitrogen atoms (C–O and C–N). The remaining aromatic carbon signals appeared in the region δ 115.98-124.30 ppm (Table-3). The methoxy carbon resonated at approximately δ 56 ppm, while the signal observed around δ 39.5 ppm originated from the DMSO-$d_6$ solvent peak [44].

**Mass spectral analysis:** The ESI-MS spectrum of the ligand ($H_2L$) exhibited a prominent molecular ion peak at *m/z* 410.1, which also served as the base peak and was in excellent agreement with its calculated molecular mass of 410.85 (Fig. 4a). The HRMS spectrum of CuL complex (Fig. 4b) displayed a molecular ion peak at *m/z* 473.1000, consistent with the expected molecular mass of 472.27. Similarly, the HRMS spectrum of NiL complex (Fig. 4c) showed a molecular ion peak at *m/z* 467.0295, closely matching the calculated molecular mass of 467.53. In addition, a prominent peak observed at *m/z* 489.0112 was assigned to the sodium adduct ion, $[M+Na]^+$ ion, further supporting the proposed molecular structure of the Ni(II) complex.

**Thermal studies:** The thermal stability of the NiL and CuL complexes was investigated by thermogravimetric analysis (TGA) and differential scanning calorimetry (DSC) under a $N_2$ atmosphere and the corresponding thermograms are shown in Fig. 5a-b. The TGA curve of the NiL complex (Fig. 5a) exhibited an initial weight loss of approximately 4% below 100 ºC, which is attributed to the removal of moisture and physically adsorbed water molecules. This observation is supported by the broad endothermic peak observed in the DSC

TABLE-2
KEY IR BANDS ($cm^{-1}$) OF THE LIGAND $H_2L$ AND ITS METAL(II) COMPLEXES

| Ligand/complex | ν(C=N) | ν(C=C) | $\nu(C–O)_{phenolic}$ | ν(M–O) | ν(M–N) |
|---|---|---|---|---|---|
| $H_2L$ | 1611 | 1575 | 1252 | – | – |
| NiL | 1605 | 1544 | 1248 | 537 | 447 |
| CuL | 1609 | 1539 | 1242 | 523 | 441 |

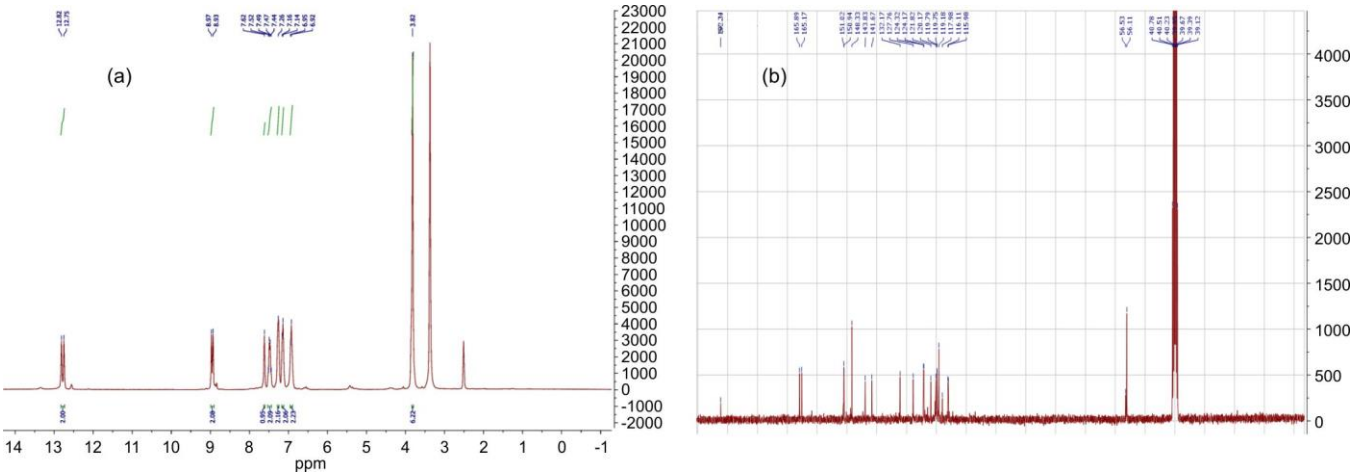


Fig. 3. (a) $^1$H NMR and (b) $^{13}$C NMR spectra of $H_2L$

TABLE-3
PROTON MAGNETIC RESONANCE SPECTRAL DATA (δ, ppm) OF THE SCHIFF BASE ($H_2L$)

| $^1$H NMR data | | $^{13}$C NMR data | |
|---|---|---|---|
| Functional group assigned | Chemical shift ($\delta_H$, ppm) | Group assigned | Chemical shift ($\delta_C$ (ppm) |
| Phenolic –OH | 12.82, 12.75 | Aromatic carbons (-C-O, C-N) | 151.02, 150.94, 148.33, 143.83, 141.67 |
| Azomethine -HC=N | 8.97, 8.93 | Azomethine -HC=N | 165.89, 165.17 |
| Aromatic rings protons | 6.92-7.62 | Aromatic methines (=CH, =C, =C-Cl) | 132.17, 127.76, 124.32, 124.17, 121.82, 120.17, 119.79, 119.75, 119.18, 117.98, 116.11, 115.98 |
| -$OCH_3$ | 3.82 | -$OCH_3$ | 56.53, 56.11 |

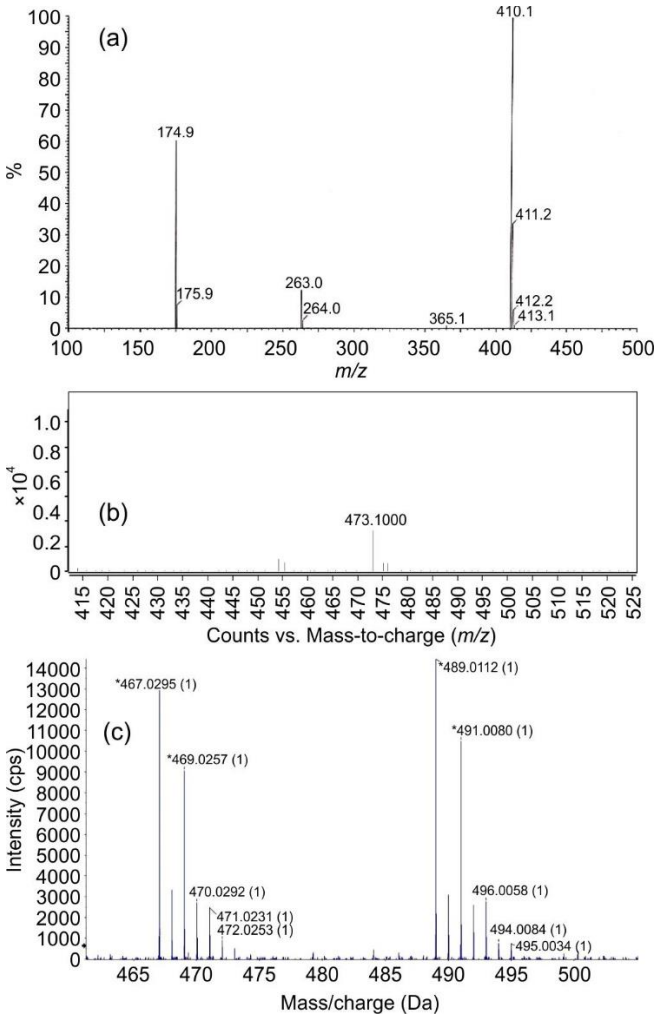


Fig. 4. (a) ESIMS spectra of $H_2L$, (b) HRMS spectra of CuL and (c) HRMS spectra of NiL

curve (Fig. 5b) within the 70-100 ºC temperature range. A stable weight plateau was observed between 120 and 210 ºC, indicating good thermal stability of the complex over this interval. Upon further heating, a significant weight loss of approximately 13% occurred between 210 and 325 ºC, corresponding to the decomposition of the organic ligand framework. This decomposition is accompanied by a pronounced endothermic peak around 250 ºC, indicating decomposition of the coordination bonds. An exothermic peak observed near 325 ºC is attributed to oxidation of the decomposition products. Above 350 ºC, the complex underwent gradual decomposition, leaving a final residual mass of approximately 12.4%.

The CuL complex exhibited a similar initial weight loss of approximately 4.1% at lower temperatures (Fig. 5a), arising from the removal of moisture and entrapped solvent molecules. This process is reflected by a broad endothermic region in the corresponding DSC curve (Fig. 5b). In contrast to the NiL complex, CuL underwent rapid thermal decomposition between 180 and 220 ºC, accompanied by a sharp decrease in mass from approximately 13% to 15.8%. This rapid weight loss coincides with a distinct endothermic peak at around 200 ºC, indicating the fast decomposition of the copper complex. At higher temperatures, continuous mass loss was observed, resulting in a final residual mass of approximately 29%. Unlike the NiL complex, no exothermic peak was detected for CuL, suggesting continuous decomposition without any detectable phase transition or crystallization process [45].

**Powder XRD studies:** The PXRD patterns of the synthesised complexes were recorded over a 2θ range of 10-90º (Figs. 6a-b). The NiL complex exhibited prominent diffraction peaks at approximately 2θ = 14.5º and 25.6º, along with several less intense reflections at higher angles. Similarly, the CuL complex showed distinct diffraction peaks at approximately 2θ = 10.2º, 19.8º, 26.4º and 28.1º, indicating the presence of well-defined crystalline domains. The sharp diffraction peaks observed for both complexes confirmed their crystalline nature. However, the presence of a broad background and diffuse scattering, particularly at higher diffraction angles, suggests the coexistence of amorphous and crystalline phases. Compared to NiL, the CuL complex exhibited a greater number of intense reflections with higher peak intensities, indicating a higher degree of crystallinity and improved structural ordering [46,47]. The mean crystallite dimensions were calculated using the following Scherrer formula:

$$D = \frac{K\lambda}{\beta \cos\theta}$$

where λ is the wavelength of X-ray used; β is the signal's FWHM, θ is the Bragg angle; K is the Scherrer constant (often 0.9) and D is the crystallite's size. The average crystallite sizes were found to be 140.76 nm for the NiL and 58.13 nm for the CuL.

**SEM analysis:** The SEM image of the NiL complex (Fig. 7a) reveals an aggregated network of elongated rod-like and needle-shaped crystallites arranged in an interwoven fibrous structure. The particles are densely packed and rand- omly oriented, indicating anisotropic crystal growth during the complexation process. In contrast, the CuL complex (Fig. 7b) exhibits a predominantly layered and plate-like morpho-logy composed of stacked flakes with relatively smooth

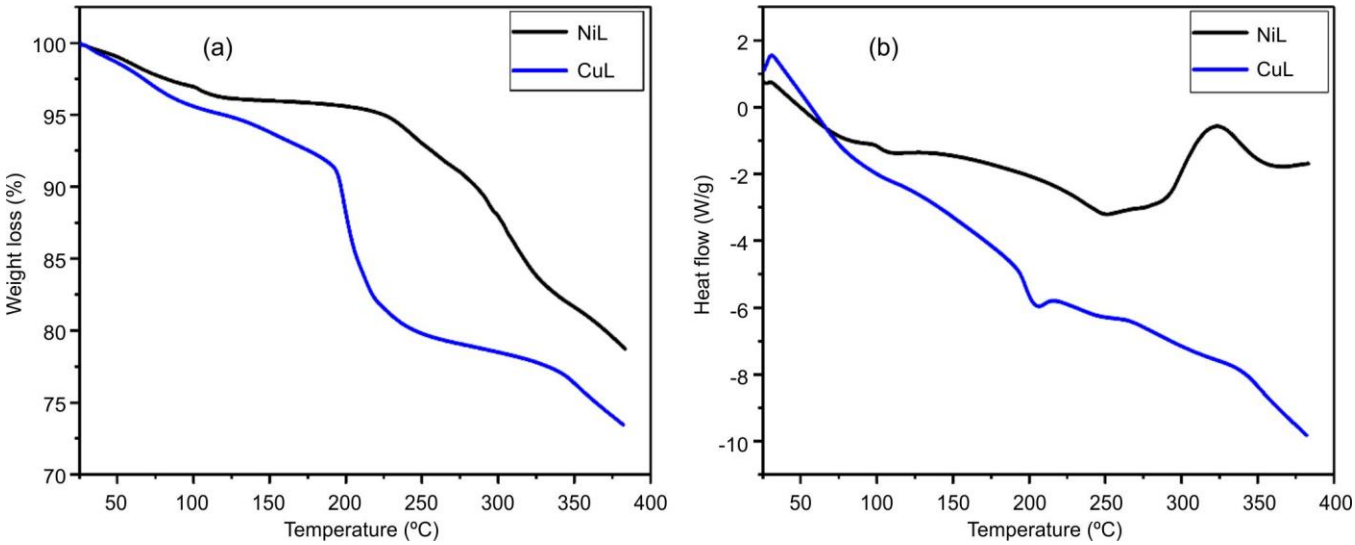


Fig. 5. (a) TGA curves of complexes NiL and CuL and (b) DSC curves of complex NiL and CuL

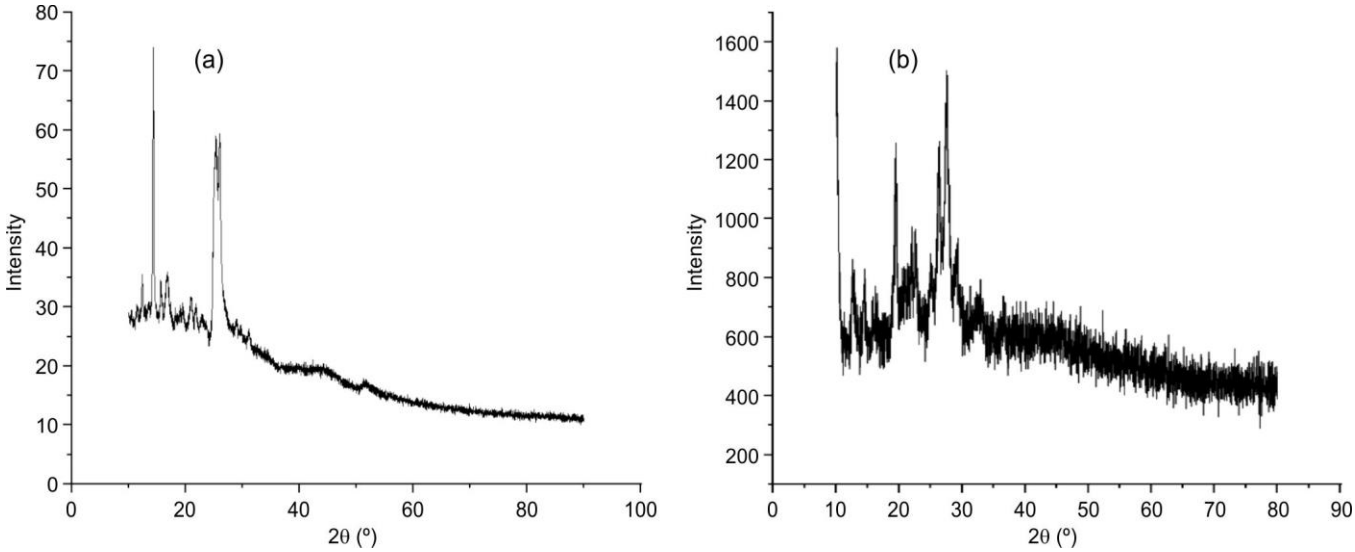


Fig. 6. XRD of (a) NiL and (b) CuL

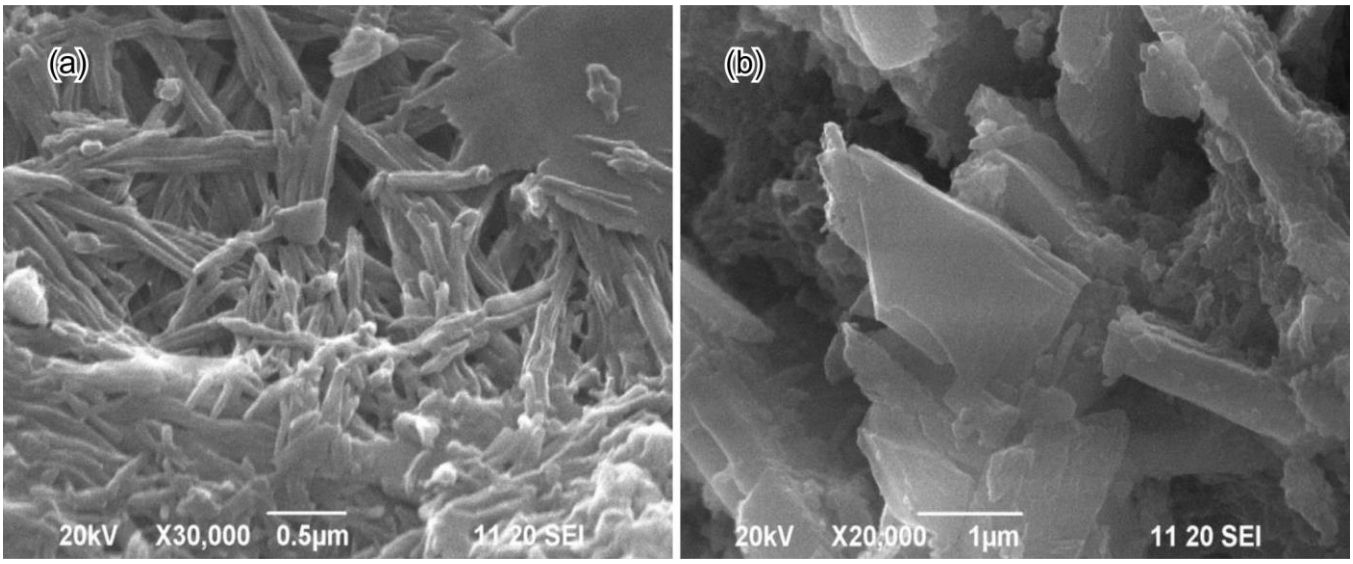


Fig. 7. SEM image of (a) NiL and (b) CuL

surfaces and well-defined edges. The observed morphology suggests the formation of compact crystalline domains within the CuL complex.

Both metal(II) complexes exhibit significant particle agglomeration, which may arise from strong intermolecular interactions and crystal packing effects commonly observed in the coordination compounds [48]. The morphological differences between NiL and CuL complexes indicate that the nature of the coordinated metal ion significantly influences the crystal growth and particle assembly. The SEM observations are in good agreement with the PXRD results, which confirmed the crystalline nature of both complexes. While NiL displays a fibrous and elongated morphology, CuL exhibits a more compact layered structure with well-developed crystalline features.

**Antimicrobial activity:** The free ligand $H_2L$ exhibited relatively weak antimicrobial activity against all tested microorganisms, producing inhibition zones of approximately 8-11 mm. Upon coordination with metal ions, a sginificant enhancement in biological activity was observed, particularly for the Cu(II) complex. CuL displayed the highest antibacterial activity among the synthesized compounds, with inhibition zone diameters of approximately 26.5, 23.0 and 26.5 mm against *E. coli*, *P. aeruginosa* and *S. aureus*, respectively. These values exceeded those obtained for the reference drug erythromycin, indicating superior antibacterial efficacy. In contrast, the Ni(II) complex exhibited moderate antibacterial activity, with inhibition zones ranging from 10-13 mm, which were generally lower than those of CuL and comparable to or slightly below those of the standard antibiotic (Table-4).

TABLE-4
ANTIMICROBIAL ACTIVITY DATA OF SCHIFF BASE LIGAND AND ITS METAL(II) COMPLEXES

| Microorganism | $H_2L$ (mm) | NiL (mm) | CuL (mm) | Standard (mm) |
|---|---|---|---|---|
| *E. coli* | 8.5±0.3 | 10.0±0.4 | 26.5±0.5 | 12.5±0.4 |
| *P. aeruginosa* | 10.0±0.3 | 12.5±0.4 | 23.0±0.5 | 15.0±0.4 |
| *S. aureus* | 10.5±0.3 | 12.0±0.4 | 26.5±0.5 | 17.5±0.4 |
| *C. albicans* | 10.0±0.3 | 10.0±0.3 | 11.0±0.4 | 34.0±0.6 |
| *A. flavus* | 8.5±0.3 | 14.5±0.4 | 13.5±0.4 | 27.0±0.5 |

In the antifungal assay, both CuL and NiL exhibited measurable inhibitory activity against *C. albicans* and *A. flavus*. However, their inhibition zones were considerably smaller than those produced by fluconazole. Among the synthesised compounds, CuL showed slightly higher activity against *C. albicans*, whereas NiL exhibited marginally better inhibition of *A. flavus*. Despite this enhancement relative to the free ligand, the antifungal activities of the metal(II) complexes remained inferior to that of the standard antifungal drug [49].

**Molecular docking studies:** Molecular docking studies were performed to evaluate the binding affinities of the Schiff base ligand ($H_2L$) and its metal(II) complexes toward selected microbial target proteins. The binding affinity values together with the nature of intermolecular interactions within the active sites were used to assess the potential antimicrobial activity of the synthesized compounds. The principal binding interactions of the metal complexes with the target proteins are shown in Fig. 8, while the corresponding docking scores are given in Table-5.

TABLE-5
DOCKING SCORE OF $H_2L$ AND ITS Ni(II), Cu(II) COMPLEXES

| Ligand/ complex | Binding energy (kcal $mol^{-1}$) | | | |
|---|---|---|---|---|
| | 1kzn | 4cl6 | 3fyv | 5fsa |
| $H_2L$ | -8.3 | -7.7 | -9.1 | -9.0 |
| NiL | -8.7 | -8.0 | -10.9 | -10.6 |
| CuL | -7.3 | -8.0 | -8.9 | -9.9 |

For the *E. coli* target protein, the CuL complex formed two hydrogen-bonding interactions with residues Gln A-135 and Gln A-72, while additional stabilization was provided through π-alkyl interactions with Met A-135, resulting in a binding affinity of approximately -8.0 kcal $mol^{-1}$ [50]. The NiL complex exhibited an even stronger interaction, with a docking score of -8.7 kcal $mol^{-1}$. In case of *P. aeruginosa*, CuL complex established a hydrogen bond with Lys B-112 and displayed a docking score of approximately -8.0 kcal $mol^{-1}$, whereas NiL showed a comparable binding affinity of -8.0 kcal $mol^{-1}$. Against the *S. aureus* target, CuL interacted with Ser X-135 and Phe X-151 through hydrogen-bonding interactions, yielding a docking score of -8.9 kcal $mol^{-1}$. Notably, NiL demonstrated the strongest binding among all tested compounds toward this protein, with a docking score of -10.9 kcal $mol^{-1}$ [51]. For the fungal target protein of *C. albicans*, the CuL complex formed hydrogen-bonding interactions with residues Cys A-470 and Thr A-311, resulting in a docking score of approximately -10.0 kcal $mol^{-1}$. The NiL complex again exhibited slightly stronger binding, with a docking score of -10.6 kcal $mol^{-1}$. Thus, both metal(II) complexes displayed significantly more favourable binding affinities than the free ligand, indicating that metal coordination enhances receptor binding.

## Conclusion

The tetradentate Schiff base ligand ($H_2L$), derived from *o*-vanillin and 4-chloro-*o*-phenylenediamine, and its Cu(II) and Ni(II) complexes were successfully synthesized and characterized using elemental analysis, spectroscopic techniques, mass spectrometry, thermal analysis and magnetic measurements. FTIR studies confirmed coordination through the azomethine nitrogen and phenolic oxygen atoms, resulting in the formation of an $N_2O_2$ donor chelation environment around the metal centers. The low molar conductance values established the non-electrolytic nature of the metal(II) complexes, while magnetic susceptibility data supported a square-planar geometry. HRMS results were consistent with the proposed molecular composition and TGA demonstrated good thermal stability of the complexes. PXRD and SEM analyses revealed the crystalline nature of the complexes, with average crystallite sizes of approximately 140.76 nm for NiL and 58.13 nm for CuL. Morphological studies showed rod-like aggregated crystallites for NiL and layered plate-like structures for CuL. Biological evaluation demonstrated that metal coordination significantly enhanced the antimicrobial activity of the ligand. Among the synthesized compounds, the CuL complex

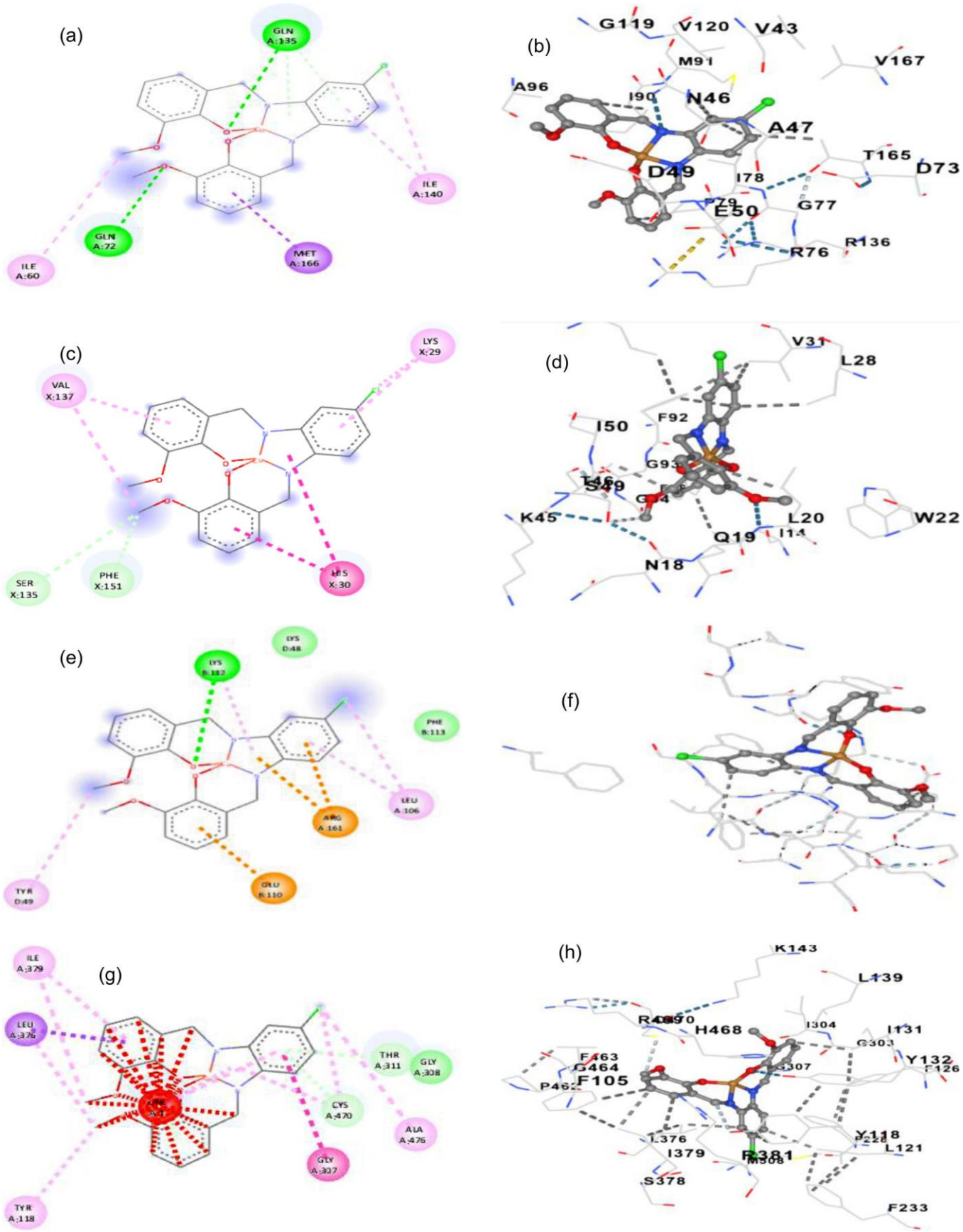


Fig. 8. Illustrative description of interactions of CuL (2-D (a) and 3-D (b)) with 1kzn, (2-D (c) and 3-D (d)) with 3Fyv, (2-D (e) and 3-D (f)) with 4Cl6 and (2-D (g) and 3-D (h)) with 5fsa

exhibited the strongest antibacterial activity against *E. coli*, *P. aeruginosa* and *S. aureus*, surpassing the activity of the reference drug erythromycin, whereas both metal(II) complexes displayed moderate antifungal activity against *C. albicans* and *A. flavus*. Molecular docking studies further supported the experimental findings by revealing favourable binding affinities and stable interactions of the complexes within the active sites of the selected microbial proteins.

## ACKNOWLEDGEMENTS

The authors are sincerely thankful to the Head, Department of Chemistry at V.S.S.D. College, Kanpur, for the facilities of research laboratory infrastructure. The authors also gratefully acknowledge IIT Kanpur, Kanpur for providing the spectral characterization facilities. Thanks are also to the University Science Instrumentation Centre (USIC), Babasaheb Bhimrao Ambedkar University (BBAU), Lucknow, for PXRD and SEM analyses. Sincere gratitude to the Department of Chemistry, Banaras Hindu University (BHU), Varanasi, for HRMS analysis and to CSIR-Central Drug Research Institute (CDRI), Lucknow, for ESI-MS measurements.

## CONFLICT OF INTEREST

The authors declare that there is no conflict of interests regarding the publication of this article.

## DECLARATION OF AI-ASSISTED TECHNOLOGIES

During the preparation of this manuscript, the authors used an AI-assisted tool(s) to improve the language. The authors reviewed and edited the content and take full responsibility for the published work.

## REFERENCES

1. A. Catalano, M.S. Sinicropi, D. Iacopetta, J. Ceramellab, A. Mariconda, C. Rosano, E. Scali, C. Saturnino and P. Longo, *Appl. Sci.*, **11**, 6027 (2021); https://doi.org/10.3390/app11136027
2. M. Pervaiz, S. Sadiq, A. Sadiq, U. Younas, A. Ashraf, Z. Saeed, M. Zuber and A. Adnan, *Coord. Chem. Rev.*, **447**, 214128 (2021); https://doi.org/10.1016/j.ccr.2021.214128
3. P.G. Cozzi, *Chem. Soc. Rev.*, **33**, 410 (2004); https://doi.org/10.1039/B307853C
4. T. Vijayan, J. Kim, M. Azam, S.I. Al-Resayes, A. Stalin, B.S. Kannan, A. Jayamani, A. Ayyakannu and S. Nallathambi, *Appl. Organomet. Chem.*, **36**, e6542 (2022); https://doi.org/10.1002/aoc.6542
5. D.B. Boyd, *J. Med. Chem.*, **26**, 1010 (1983); https://doi.org/10.1021/jm00361a013
6. K.F. Ansari and C. Lal, *Eur. J. Med. Chem.*, **44**, 2294 (2009); https://doi.org/10.1016/j.ejmech.2008.01.022
7. P. Bey and J.P. Vevert, *Tetrahedron Lett.*, **18**, 1455 (1977); https://doi.org/10.1016/S0040-4039(01)93073-4
8. A.N. Kursunlu, E. Guler, F. Sevgi and B. Ozkalp, *J. Mol. Struct.*, **1048**, 476 (2013); https://doi.org/10.1016/j.molstruc.2013.06.017
9. L.N. Obasi, G.U. Kaior, L. Rhyman and P. Ramasami, *J. Mol. Struct.*, **1120**, 180 (2016); https://doi.org/10.1016/j.molstruc.2016.05.037
10. M.A. Malik, O.A. Dar, P. Gull, M.Y. Wani and A.A. Hashmi, *MedChemComm*, **9**, 409 (2018); https://doi.org/10.1039/C7MD00526A
11. M.S. Alhussaini, A.A.I. Alyahya and A.A. Al-Ghanayem, *Dyes Pigments*, **243**, 113040 (2025); https://doi.org/10.1016/j.dyepig.2025.113040
12. D. Sudha, S. Vairam, S. Sarathbabu, N.S. Kumar, R. Sivasamy and S.J. Kirubavathy, *J. Coord. Chem.*, **74**, 2701 (2021); https://doi.org/10.1080/00958972.2021.1981302
13. S. Yasmeen, S.H. Sumrra, M.S. Akram and J.H. Chohan, *J. Enzyme Inhib. Med. Chem.*, **32**, 106 (2017); https://doi.org/10.1080/14756366.2016.1238363
14. R. Shah and P.K. Verma, *BMC Chem.*, **13**, 54 (2019); https://doi.org/10.1186/s13065-019-0569-8
15. D. Puthran, B. Poojary, N. Purushotham, N. Harikrishna, S.G. Nayak and V. Kamat, *Heliyon*, **5**, e02233 (2019); https://doi.org/10.1016/j.heliyon.2019.e02233
16. A. Hassan and A. Said, *Adv. J. Chem. A*, **4**, 87 (2020); https://doi.org/10.22034/AJCA.2021.266876.1235
17. M.A. Todarwal, R.S. Bendre and S. Karimkha, *Eur. J. Chem.*, **15**, 128 (2024); https://doi.org/10.5155/eurjchem.15.2.128-142.2543
18. H.M. Aly, M.E. Moustafa, M.Y. Nassar and E.A. Abdelrahman, *J. Mol. Struct.*, **1086**, 223 (2015); https://doi.org/10.1016/j.molstruc.2015.01.017
19. H. Kargar, M. Fallah-Mehrjardi, N. Dege, M. Ashfaq, K.S. Munawar, M.N. Tahir, M.A. Bajgirani and M. Sahihi, *J. Iran. Chem. Soc.*, **21**, 1561 (2024); https://doi.org/10.1007/s13738-024-03016-8
20. H. Bahron, S. Khaidir, A.M. Tajuddin, K. Ramasamy and B.M. Yamin, *Polyhedron*, **161**, 84 (2019); https://doi.org/10.1016/j.poly.2018.12.055
21. H.F. El-Shafiy, *J. Mol. Struct.*, **1166**, 348 (2018); https://doi.org/10.1016/j.molstruc.2018.04.023
22. T.H. Sanatkar, A. Khorshidi, E. Sohouli and J. Janczak, *Inorg. Chim. Acta*, **506**, 119537 (2020); https://doi.org/10.1016/j.ica.2020.119537
23. T. Kondori, N. Akbarzadeh, M. Fazli, B. Mir, M. Dusek and V. Eigner, *J. Mol. Struct.*, **1226**, 129395 (2021); https://doi.org/10.1016/j.molstruc.2020.129395
24. M. Balouiri, M. Sadiki and S.K. Ibnsouda, *J. Pharm. Anal.*, **6**, 71 (2016); https://doi.org/10.1016/j.jpha.2015.11.005
25. S. Nayab, A. Alam, N. Ahmad, S.W. Khan, D.F. Shams and M.I.A. Shah, *ACS Omega*, **8**, 17620 (2023); https://doi.org/10.1021/acsomega.2c08266
26. I.M. Kompis, K. Islam and R.L. Then, *Chem. Rev.*, **105**, 593 (2005); https://doi.org/10.1021/cr0301144
27. D. Murtinho, Z.N. da Rocha, A.S. Pires, R.P. Jiménez, A.M. Abrantes, M. Laranjo, A.C. Mamede, J.E. Casalta-Lopes, M.F. Botelho, A.A.C.C. Pais, S.C.C. Nunes, H.D. Burrows, T. Costa and M.E. Silva Serra, *Appl. Organomet. Chem.*, **29**, 425 (2015); https://doi.org/10.1002/aoc.3309
28. N. Raman, R. Jeyamurugan, R. Senthilkumar, B. Rajkapoor and S.G. Franzblau, *Eur. J. Med. Chem.*, **45**, 5438 (2010); https://doi.org/10.1016/j.ejmech.2010.09.004
29. P. Subbaraj, A. Ramu, N. Raman and J. Dharmaraja, *J. Saudi Chem. Soc.*, **19**, 207 (2015); https://doi.org/10.1016/j.jscs.2014.05.002
30. H.E. Hashem, A. Nath and A. Kumer, *J. Mol. Struct.*, **1250**, 131915 (2022); https://doi.org/10.1016/j.molstruc.2021.131915
31. K. Nakamoto, Infrared and Raman Spectra of Inorganic and Coordination Compounds, Part B: Applications in Coordination, Organometallic and Bioinorganic Chemistry, John Wiley & Sons (2009).
32. A.A.M. Belal, I.M. El-Deen, N.Y. Farid, R. Zakaria and M.S. Refat, *Spectrochim. Acta A Mol. Biomol. Spectrosc.*, **149**, 771 (2015); https://doi.org/10.1016/j.saa.2015.05.005
33. L.H. Abdel-Rahman, R.M. El-Khatib, L.A.E. Nassr and A.M. Abu Dief, *J. Mol. Struct.*, **1040**, 9 (2013); https://doi.org/10.1016/j.molstruc.2013.02.023
34. M. Alias, H. Kassum and C. Shakir, *J. Assoc. Arab Univ. Basic Appl. Sci.*, **15**, 28 (2014); https://doi.org/10.1016/j.jaubas.2013.03.001
35. C. Gautam, A. Singh, A. Singh, A.K. Singh, V.K. Sharma and P. Kumar, *J. Mol. Struct.*, **1243**, 130928 (2021); https://doi.org/10.1016/j.molstruc.2021.130928

36. M.S. Nair and R.S. Joseyphus, *Spectrochim. Acta A Mol. Biomol. Spectrosc.*, **70**, 749 (2008); https://doi.org/10.1016/j.saa.2007.09.006
37. P. Gluvchinsky, G.M. Mockler and E. Sinn, *Spectrochim. Acta A*, **33**, 1073 (1977); https://doi.org/10.1016/0584-8539(77)80156-6
38. A. Bigotto, G. Costa, G. Mestroni, G. Pellizer, A. Puxeddu, E. Eisenhofer, L. Stefani and G. Tauzher, *Rev.*, **4**, 41 (1970); https://doi.org/10.1016/0073-8085(70)80011-0
39. E. Yousif, A. Majeed, K. Al-Sammarrae, N. Salih, J. Salimon and B. Abdullah, *Arab. J. Chem.*, **10**, S1639 (2017); https://doi.org/10.1016/j.arabjc.2013.06.006
40. A. M. Tajuddin, H. Bahron, R. M. Hanafiah, N. Ibrahim, H.-K. Fun and S. Chantrapromma, *Acta Cryst. Sect. E: Struct. Rep. Online*, **70**, 252 (2014); https://doi.org/10.1107/S1600536814020546
41. H. Kargar, A.A. Ardakani, M.N. Tahir, M. Ashfaq and K.S. Munawar, *J. Mol. Struct.*, **1233**, 130112 (2021); https://doi.org/10.1016/j.molstruc.2021.130112
42. K.R. Joshi, A.J. Rojivadiya and J.H. Pandya, *Int. J. Inorg. Chem.*, **2014**, 412 (2014); https://doi.org/10.1155/2014/817412
43. J.H. Pandya, R.N. Jadeja and K.J. Ganatra, *J. Saudi Chem. Soc.*, **18**, 190 (2014); https://doi.org/10.1016/j.jscs.2011.06.010
44. K. Misganaw, P. Thillairasu, G. Shumi, H. Debebe and S. Berhanu, *Bull. Chem. Soc. Ethiop.*, **38**, 1275 (2024); https://doi.org/10.4314/bcse.v38i5.7
45. P. Mahadeva and H.D. Revanasiddappa, *Biointerface Res. Appl. Chem.*, **14**, 19 (2024); https://doi.org/10.33263/BRIAC141.019.
46. E.M. Abdalla, S.S. Hassan, H.H. Elganzory, S.A. Aly and H. Alshater, *Molecules*, **26**, 5851 (2021); https://doi.org/10.3390/molecules26195851
47. H.H. Elganzory, S.S. Hassan, S.A. Aly and E.M. Abdalla, *Bioinorg. Chem. Appl.*, **2006**, 451 (2022); https://doi.org/10.1155/2022/2006451
48. S.N. Melnikov, K.A. Lyssenko, I.V. Ananyev and I.L. Eremenko, *Russ. Chem. Bull.*, **66**, 1550 (2017); https://doi.org/10.1007/s11172-017-1923-4
49. A.M. Hassan, A.O. Said, B.H. Heakal, A. Younis, W.M. Aboulthana and M.F. Mady, *ACS Omega*, **7**, 32418 (2022); https://doi.org/10.1021/acsomega.2c03911
50. W.A. Shehnaz, W.A. Siddiqui, M.A. Raza, A. Ashraf, M. Ashfaq, M.N. Tahir and S. Niaz, *J. Mol. Struct.*, **1295**, 136603 (2024); https://doi.org/10.1016/j.molstruc.2023.136603
51. G. Venkatesh, P. Vennila, S. Kaya, S. Ben Ahmed, P. Sumathi, V. Siva, P. Rajendran and C. Kamal, *ACS Omega*, **9**, 8123 (2024); https://doi.org/10.1021/acsomega.3c08526